

# Performance of the Advanced Camera for Surveys CCDs after two years on orbit.

Marco Sirianni<sup>a,b</sup>, Max Mutchler<sup>b</sup>, Mark Clampin<sup>c</sup>, Holland Ford<sup>d</sup>, Garth Illingworth<sup>e</sup>, George Hartig<sup>b</sup>, Doug van Orsow<sup>b</sup> and Thomas Wheeler<sup>b</sup>.

<sup>a</sup>European Space Agency; <sup>b</sup>Space Telescope Science Institute; <sup>c</sup>Goddard Space Flight Center; <sup>d</sup>Johns Hopkins University <sup>e</sup>University of California – Santa Cruz

## ABSTRACT

The Advanced Camera for Surveys (ACS), installed in the Hubble Space Telescope (HST) in March 2002, comprises three cameras: the Wide Field Camera (WFC), designed for deep near-IR survey imaging programs; the High Resolution Camera (HRC), a high angular resolution imager which fully samples the HST full spread function (PSF) in the visible; and the Solar Blind Camera (SBC), a far-UV imager. The WFC and HRC employ CCD detectors. Their performances are affected by the on-going damage due to the space radiation environment where they operate. We present an overview of the performance of the ACS CCD detectors, based on the first two years of flight science operations. We analyze the evolution with time of the basic detector performance that are subjected to degradation due to the on-going radiation damage. Comparison is made with ground testing prediction and with the amount of performance degradation seen in other CCD detectors on board of HST.

Keywords: HST, ACS, HRC, WFC, CCDs, CTE, Dark Rate, Hot Pixels, Radiation Damage

## 1. Introduction

The Advanced Camera for Surveys (ACS) is a third generation instrument for the Hubble Space Telescope's (HST) second decade of science operations. It was installed during the fourth HST servicing mission (SM3B), in March 2002 and replaced a first generation axial bay instrument, the Faint Object Camera (FOC). ACS provides HST with a powerful complement of three new imagers, the Wide Field Camera (WFC), the High Resolution Camera (HRC) and the Solar Blind Camera (SBC). The WFC is a high throughput (48% at 660 nm, including the HST optical telescope assembly), wide field (202" x 202"), optical and I-band camera that is half critically sampled at 500 nm. The HRC is critically sampled at 500 nm, and has a 26" x 29" field of view and 28% total throughput at 630 nm. The SBC is a far ultraviolet, solar-blind camera that has a relatively high throughput (4.9% at 126 nm) over a 31" x 35" field of view. Ford et al. (1996)<sup>1</sup> described in detail the design of the camera and its elements. Two of the three cameras, the WFC and the HRC employ CCD detectors<sup>2,3</sup>. The SBC employs a photon-counting MAMA detector whose performance has been described in detail by Tran et al. (2002)<sup>4</sup>.

Ford et al. (2002)<sup>5</sup> (and reference therein) present an overview of the initial on-orbit performance and characterization of the camera. Sirianni et al. (2003)<sup>6</sup> present the on-orbit characterization of the ACS CCD detectors and the comparison of the inflight result with pre-launch calibration data. Clampin et al. (2004)<sup>7</sup> present an overview of the ACS CCD detectors based on the first year of flight science operations. In this paper we will focus on the performance aspects of the ACS CCD detectors which show a temporal variation due to the on-going radiation damage: read noise, dark current, hot pixel population and Charge Transfer Efficiency (CTE).

## 2. ACS CCD: Architecture

### 2.1. WFC

The focal plane of the WFC consists of two butted SITe 2048 x 4096 pixel CCDs. The CCD design is derived from the three-side buttable SITe commercial 4096x2048 array (ST-002A). However, due to concerns regarding degradation of charge transfer efficiency (CTE), due to the radiation environment in HST's low earth orbit, the configuration of the

commercial design has been specifically modified for ACS. The ACS ST-008A devices have the serial register along the 4096 pixels edge, and reads out through an amplifier at each end. This chip is designed to be buttable along only one edge making the 2x1 mosaic possible. The new design reduces the readout to 2048 parallel and 2048 serial shifts for each quadrant of the 4096 x 4096 mosaic. Although the 2-amps readout is the default configuration, each chip can also be read out through a single amplifier, thus increasing the readout time. There are 24 additional extended pixels (physical overscan) on each side of the serial readout register, just before each amplifier. The WFC data also contain a virtual overscan, 20 rows on the top of the chip, obtained overclocking after the readout of the last CCD row. The WFC focal plane package has been described in detail in Clampin et al. (1998)<sup>2</sup>. The cosmetics of the WFC flight CCD has been discussed in Sirianni et al. (2002)<sup>3</sup> and the basic in flight performance is reported in Sirianni et al (2003)<sup>6</sup>.

<b>Imaging Area</b>	2 x 4096 x 2048	<b>Pixel- Size</b>	15 $\mu\text{m}$ x 15 $\mu\text{m}$
<b>Architecture</b>	3-phase backside-thinned MPP (only during integration)	<b>AR coating</b>	SITE VIS-AR Coating
<b>Serial Register</b>	1 in each device	<b>Amplifier</b>	2 in each device
<b>Full Well</b>	$\sim 80,000$ e- (MPP)		
<b>Mini-channel</b>	3 $\mu\text{m}$ , parallel and serial register	<b>Clocking rate</b>	3212 $\mu\text{sec}$ (par.) 22 $\mu\text{sec}$ (ser.)
<b>Operating Temperature</b>	-76 C (1x4-stages TEC + 4x2-stages TEC)		

Table 1: ACS/WFC CCDs specifications

## 1.2. HRC

The HRC detector is a single 1024 x 1024 pixel CCD manufactured by SITe. It is based on the backside illuminated STIS 1024x1024 21  $\mu\text{m}$  CCD but it differs in the backside processing that has been optimized for the near UV. This device has four output amplifiers, one at each end of the two serial registers. The array can be therefore divided into 512 x 512 quadrants to minimize the readout time and the CTE loss. The default configuration is a single amplifier readout. There are 19 additional extended pixels on each side of the serial register, just before each amplifier.

The HRC data also contain a virtual overscan, 20 rows on top of the chip, obtained overclocking after the readout of the last CCD row. The HRC focal plane package is described in Clampin et al. (1998)<sup>2</sup>. The initial on orbit characterization is presented in Sirianni et al (2003)<sup>6</sup>.

<b>Imaging Area</b>	1 x 1024 x 1024	<b>Pixel- Size</b>	21 $\mu\text{m}$ x 21 $\mu\text{m}$
<b>Architecture</b>	3-phase backside-thinned MPP	<b>AR coating</b>	SITe UV-AR Coating
<b>Serial Register</b>	2 in each device	<b>Amplifier</b>	2 in each device
<b>Full Well</b>	$\sim 150,000$ e- (MPP)		
<b>Mini-channel</b>	3 $\mu\text{m}$ , parallel and serial register	<b>Clocking rate</b>	1892 $\mu\text{sec}$ (par.) 22 $\mu\text{sec}$ (ser.)
<b>Operating Temperature</b>	-81 C (1x4-stages TEC )		

Table 2: ACS/HRC CCDs specifications

## 3. Bias Level and Readout noise

In order to properly calibrate the scientific observations with ACS and to monitor the detectors performances, bias frames are acquired daily for all supported modes<sup>8</sup>. Every two weeks multiple bias frames are combined together to remove the cosmic rays accumulated during the readout time ( $\sim 100$  sec for WFC,  $\sim 27$  sec for HRC) and to enhance the signal-to-noise ratio of the bias pattern. Bias frames have three different sections that can be used to estimate the bias level and readnoise: the image area, the physical overscan and the virtual overscan. In this section we will primarily

discuss the bias level and readnoise for the default readout and gain configurations (WFC: 4 amps readout, gain=1e-/DN; HRC: 1 amp readout, gain=2e-/DN). More detailed information on all modes are available in Sirianni et al (2003)<sup>6</sup>.

### 3.1. Bias Level

- **WFC** – Each quadrant has two overscan regions: a 24-pixel wide leading physical overscan at columns 1-24 and a 20 rows wide virtual overscan at rows 2049-2068. Due to a horizontal ramp in the first columns of the leading physical overscan only the last 6 columns adjacent to the active area are used for the measurement of the bias level. The stability of the bias level in the leading physical overscan in the first three months after the launch have been reported in Sirianni et al (2003)<sup>6</sup>. Each month the Thermo Electric Coolers (TECs) are turned off to allow the CCD to warp up to the ambient temperature (~ 20 C) and anneal hot pixels created by the radiation damage (see section 5). After a period between 10 to 16 hours the focal plane is brought back to its nominal temperature and bias frames are acquired. The bias frames acquired within a few hours after the annealing period show a bias level higher than the last frame taken just before the anneal. Only after a few hours the bias level settles down to the original level. Figure 1 shows the temporal evolution of the bias level in the leading physical overscan for the four WFC amplifiers at gain 1. The annealing dates are marked with vertical lines and the increased bias level after each line is clearly visible. These variations in the bias level are not a concern for calibration purpose because the leading overscan and the image area show the same trend. If we do not consider this monthly feature, the bias level in all four quadrants has been decreasing with time with a slightly higher rate in the first year than in the second one. As shown in Figure 1, in addition to the monthly feature, the bias level of amp-B shows an intrinsic scatter of about 20 DN (peak to peak) at any given time. Since the bias level in the active area changes accordingly, and with the same amplitude, this fluctuation does not represent a concern for the calibration of scientific observations. It is interesting to note the effects of sharing some of the off-chip electronics between opposite quadrants (A-D and B-C) on the bias level. The bias level in amps A and D shows less scatter than the other two amplifiers; moreover in these two quadrants there has been a departure from a steady decreasing trend between day 400 and 600. Such a feature is not visible in quadrants B and C, probably due to the intrinsic noise in the bias level distribution. A detailed analysis of the WFC bias frames and comparison between the bias level in the three different regions is presented in a forthcoming publication<sup>9</sup>.
- **HRC** - The bias level in the HRC CCD shows the same trend observed in WFC CCDs (figure 2).

### 3.2. Read Noise

- **WFC** - We measured the read noise level in the active area and overscan regions for all the amplifiers at the default gain settings. On June 29, 2003, just after a transit through the South Atlantic Anomaly (SAA) the readnoise in Amp A changed from ~4.9 to ~5.9 e- rms. Although the telemetry did not show any anomaly in any component of the camera, it is likely that the read noise jump was due to some sort of radiation damage. Amp A is the only amplifier that showed any anomaly. The amplitude of the variation (~ 1 e-) has been the same for gain 1 and 2. After the following anneal date the readnoise dropped to ~5.5 and it has been constant for 27 days. After the following two anneal cycles the read noise reached stability at ~ 5.6 e- rms, approximately 0.7 e- higher than its initial value and it has remained constant since then. Figure 3 shows the read noise in the image area for amplifier A during the “instability” period. The readnoise of all the other amplifiers has been very stable since launch with post-launch figures almost unchanged from pre-launch measurements made during ground testing, as shown in Table 3. Even with a slightly higher read noise in Amp A most of the WFC broadband science observations are sky limited while narrowband observations are primarily read noise limited.
- **HRC** – The read noise is monitored only for the default readout amplifier C at the default gain setting (2 e-/DN). No variations have been observed with time. The read noise measured in the image area (4.80 +/- 0.12) is in agreement with the readnoise measured in the two overscan regions and it is comparable to the pre-flight 4.74 e-value.

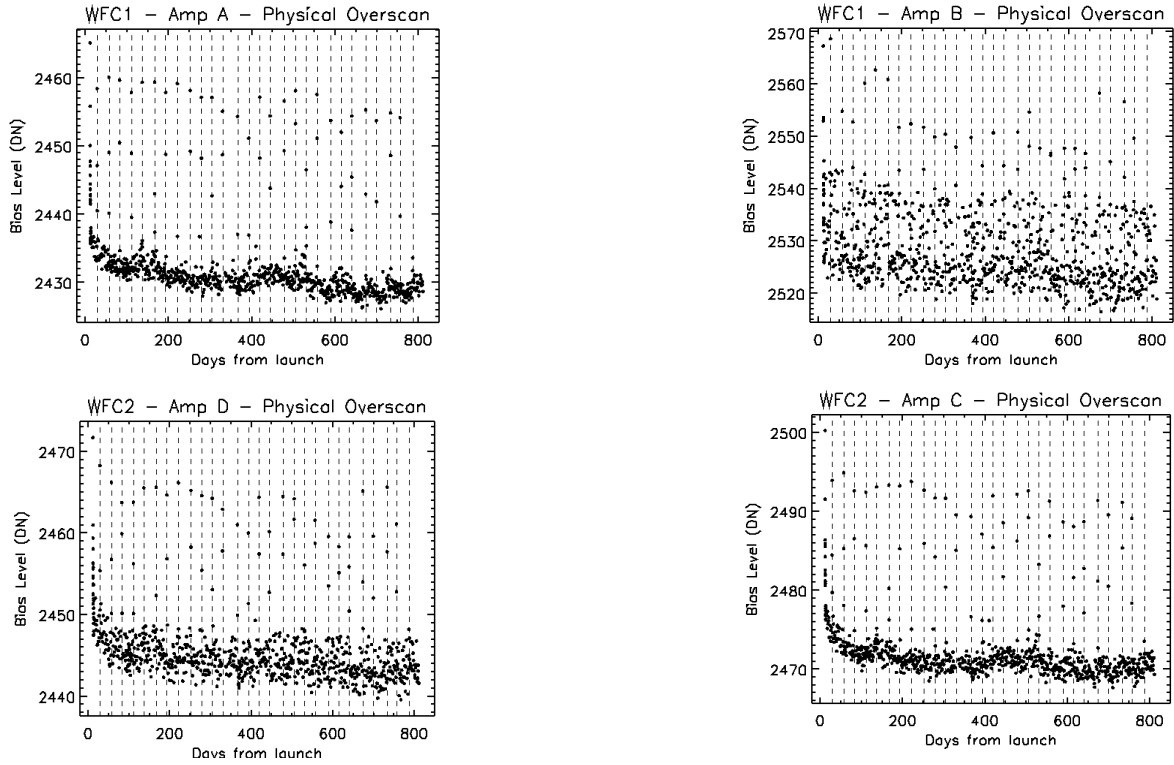


**Figure 1.** Bias level vs time for the WFC CCDs (gain=1). The vertical dashed lines mark the annealing dates.

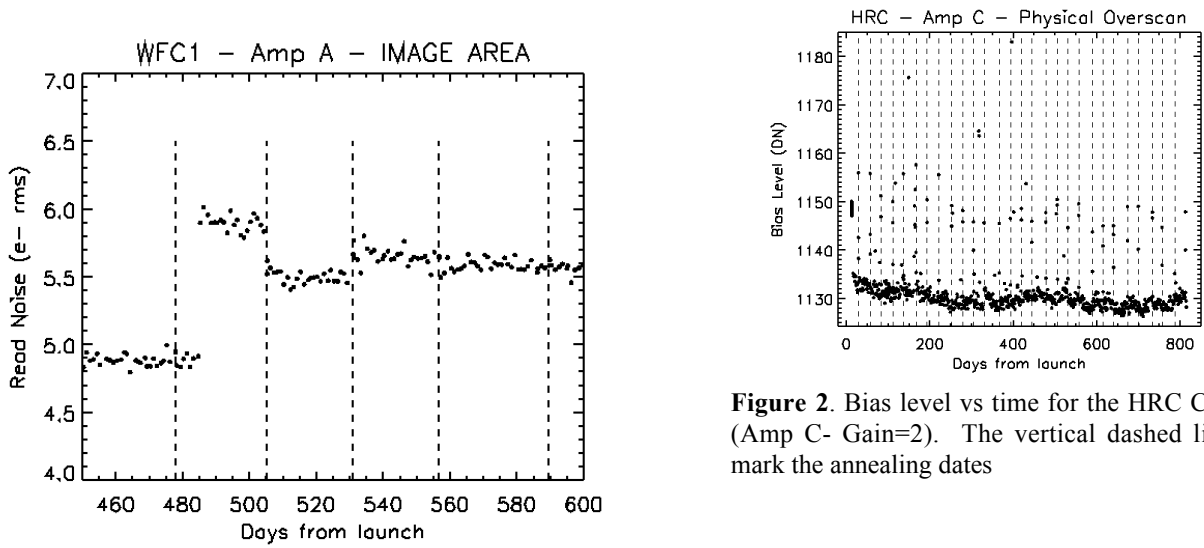


**Figure 2.** Bias level vs time for the HRC CCD (Amp C- Gain=2). The vertical dashed lines mark the annealing dates

**Figure 3:** The read noise jump in WFC- AMP A that occurred on June 29, 2003. The vertical dashed lines indicate the annealing dates.

Chip	Amp	Gain <sup>a</sup>	Ground	Flight			
				Physical overscan	Virtual overscan.	Image area	
WFC - 1	A	1.000	4.8 ± 0.1	4.60 ± 0.20 <sup>b</sup> 5.28 ± 0.11 <sup>c</sup>	4.94 ± 0.11 <sup>b</sup> 5.65 ± 0.11 <sup>c</sup>	4.87 ± 0.05 <sup>b</sup> 5.57 ± 0.05 <sup>c</sup>	
		2.002	5.3 ± 0.1	4.96 ± 0.10 <sup>b</sup> 5.59 ± 0.14 <sup>c</sup>	5.27 ± 0.10 <sup>b</sup> 5.92 ± 0.11 <sup>c</sup>	5.21 ± 0.04 <sup>b</sup> 5.84 ± 0.08 <sup>c</sup>	
	B	0.972	4.7 ± 0.1	4.45 ± 0.09	4.74 ± 0.12	4.70 ± 0.04	
		1.945	5.1 ± 0.1	4.74 ± 0.09	5.02 ± 0.11	4.98 ± 0.04	
	WFC -2	C	1.011	5.2 ± 0.1	4.85 ± 0.10	5.28 ± 0.14	5.18 ± 0.05
			2.028	5.4 ± 0.1	5.05 ± 0.10	5.43 ± 0.12	5.35 ± 0.04
D		1.018	4.7 ± 0.1	4.53 ± 0.08	4.85 ± 0.11	4.80 ± 0.03	
		1.994	5.1 ± 0.1	4.99 ± 0.08	5.30 ± 0.10	5.27 ± 0.04	

**Table 3:** Read noise for WFC amplifiers

<sup>a</sup> Gain values from Gilliland (2004); <sup>b</sup> before June, 29 2003; <sup>c</sup> after June, 29 2003.

#### 4. Dark Current

All ACS CCDs are buried channel devices which have a shallow n-type layer implanted below the surface to store the collected signal charge away from the traps associated with the Si-SiO<sub>2</sub> interface. Moreover ACS CCDs are operated in MPP mode so that the silicon surface is inverted and the surface dark current is therefore suppressed. WFC CCDs are operated in MPP mode only during integration, so the total dark current figure for WFC includes a small component of surface dark current accumulated during the readout time.

Like all CCDs operated in a low earth orbit radiation environment the ACS CCDs are subject to radiation damage by energetic particles in the radiation belt. Ionization damage and displacement damage are the two groups of damages caused by protons in silicon. The MPP mode is very effective in mitigating the damage due to ionization such as the generation of surface dark current due to the creation of trapping states in the Si-SiO<sub>2</sub> interface. Although only a minor fraction of the total energy is lost by a proton via non-ionizing energy loss, the displacement damage can cause significant performance degradation in CCDs, by decreasing the CTE, increasing the average dark current, and by introducing pixels with very high dark current (hot pixels).

Displacement damage to the silicon lattice occurs mostly due to the interaction between low energy protons and silicon atoms. The generation of phosphorous-vacancy centers introduces an extra level of energy between the conduction band and the valence band of the silicon. New energetic levels in the silicon bandgap have the direct effect of increasing the dark current as a result of carrier generation in the bulk depletion region of the pixel. As a consequence the dark current of CCDs operated in a radiative environment is predicted to increase with time. Ground testing of WFC devices, radiated with a cumulative fluence equivalent to 2.5 and 5 years of on-orbit exposure, predicted a linear growth of ~ 1.5 e-/pix/hr/yr. During the testing the WFC CCDs were operated at -81 C, about 5 degrees cooler than the on-orbit operating temperature.

The dark current in ACS CCDs is monitored daily with the acquisition of four 1000 seconds dark frames. Dark frames are used to create reference files for the calibration of scientific images and to track and catalog hot pixels as they evolve (See next section). The four daily frames are combined together to remove cosmic rays and to extract hot pixels information for any specific day. In order to reduce the statistical noise the dark references files are generated by combining two weeks of daily darks. The hot pixel information for a specific day is then added to the combined bi-weekly dark.

In order to study the evolution of the dark current with time we calculated the modal dark current value in the cosmic-ray free daily darks. As expected, the dark current increases with time (Fig 4). The observed dark current increases linearly with time at a rate of 1.4 and 2 e-/pix/hr/yr for WFC1 and WFC2 respectively and 1.8 for the HRC CCD. These rates are in general agreement with the ground testing prediction (Table 4). We also calculated the equivalent trend using only the dark frames acquired just after each anneal but there we found no difference. This indicates that the

majority of the pixels, which are getting slightly “warmer” with time do not benefit from the anneal cycles as much as hotter pixels.

It is interesting to compare the evolution of dark current in other CCDs currently operated on board of HST which are exposed to the same radiation environment (Table 4). The STIS CCD is very similar to the ACS/HRC CCD; they only differs in the AR coating, clocking rate and operating temperature. Starting from the launch in Nov 1997 the STIS CCD’s dark rate has been increasing linearly at  $\sim 3.3$  e-/pix/hr/yr until December 1999 when some instability in the readout amplifier electronic was reported. Between Dec 1999 and May 2001 the dark rate did not increase. On May 2001 the primary Side-1 electronics on STIS failed. Operations were resumed using the backup Side-2 electronics and the dark current re-started increasing with time but at a lower pace ( $\sim 2.2$  e-/pix.hr/yr). The STIS Side-2 electronics do not have a working CCD temperature controller. As a consequence the CCD temperature cannot be held constant, but fluctuates with the temperature of the spacecraft environment. As a consequence the dark rate is also fluctuating. However, since the current of the TEC is fixed at a higher value than the typical value required to hold the  $-83\text{C}$  set point on Side 1, the detector is often cooler than it was during Side-1 operations<sup>10</sup>.

The WFPC2 CCDs are thick 800x800 front-side illuminated devices produced by Loral and are operated at  $-88\text{C}$ . The dark current evolution with time has been presented in Mack et al. (2001)<sup>11</sup>. In the first five years of operation, the dark rate growth for the four different devices has been between 2.0 and 3.3 e-/pix/hr/yr. However, since summer 1998, no further increase in the dark rate has been observed. The right panel in figure 5 shows the dark current for the central region of the WFPC2-PC CCD. The other three WFPC2 CCDs show a similar trend. At the moment there is no explanation for this behavior. Initial hypotheses<sup>11</sup> suggesting that the lower dark rate increase could have been linked to the reduced cosmic ray rates due to a maximum of solar activity are likely incorrect because the WFPC2 dark current remained constant even years after the solar maximum.

Finally ground testing on radiated Marconi device for WFC3 indicates that the expected dark rate degradation in the HST orbit is similar to the one observed in ACS devices<sup>12</sup>.

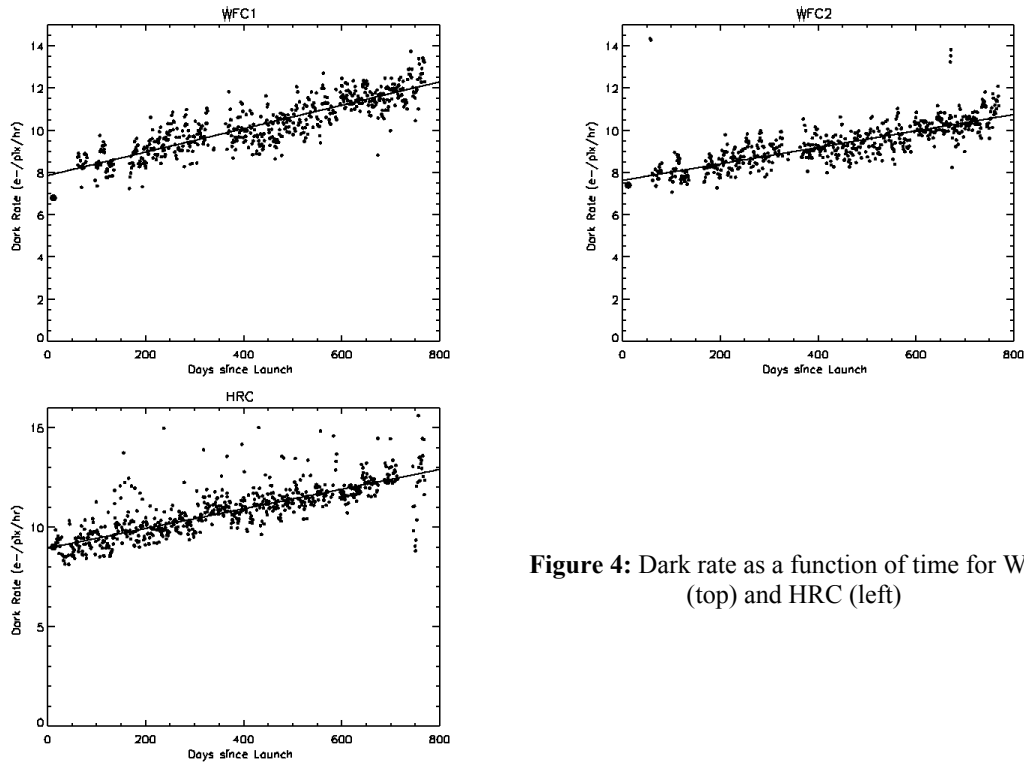


**Figure 4:** Dark rate as a function of time for WFC (top) and HRC (left)

	ACS/WFC	ACS/HRC	STIS	WFPC2	WF3
<b>Predicted (rad. Test)</b> (e-/pix/hr/yr)	1.5 (-81 C)	<i>n.a</i>	<i>n.a</i>	<i>n.a</i>	1.4 (-83 C)
<b>On-orbit (e-/pix/hr/yr)</b>	1.4 – wfc1 2.0 – wfc2	1.8	3.3 (side 1) 2.2 (side 2)	2.0-3.3 (0-5 yr) ~ 0 (after 5 yrs)	
<b>CCD Temperature</b>	-77 C	-81 C	-83 C / (?)	-88 C	
<b>Current rate (e/pix/hr)</b>	12.5/11.0	13	21.5	27.3	

**Table 4:** Dark current evolution with time for ACS CCDs and other CCDs on board of HST.

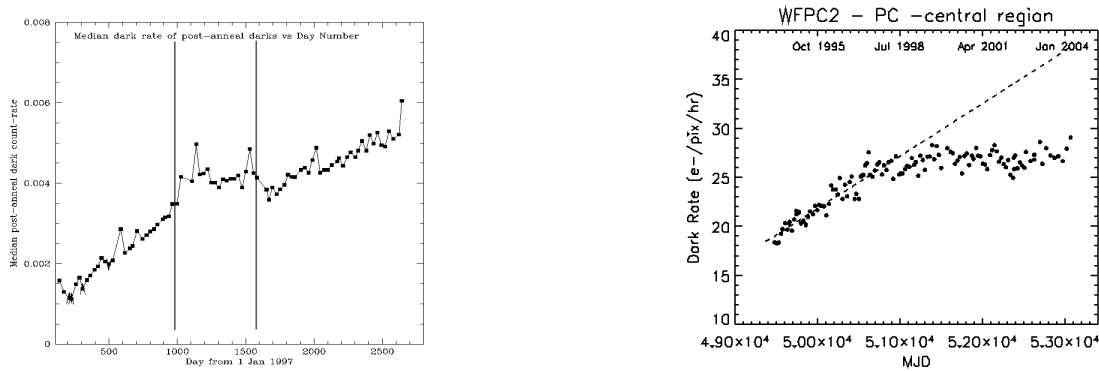
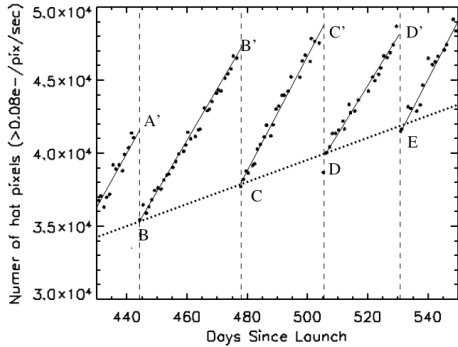


Fig 5: Dark rate evolution with time for STIS CCD (left) and for the “PC” CCD in WFPC2. The vertical lines in the plot on the left mark the beginning of the electronic instability on Side-1 (December 1999) and the beginning of operation on Side 2 (May 2001).

## 5. Hot Pixels

Frequent collection of dark frames is important to track and catalog hot pixels as they evolve. The growth of hot pixels in ACS CCDs was evaluated over the first few month of operation by Riess (2002)<sup>13</sup> selecting two different thresholds for the definition of hot pixels in WFC and HRC. In this paper we analyze the evolution of the hot pixel population over two years of annealing cycles. Hot pixels are created continuously as a result of the ongoing displacement damage on orbit. The number of new pixels that generate a dark current higher than the mean dark rate increases every day by several tenths to several hundreds depending on the threshold. Likely, most of these new hot pixels are transient. Like other CCDs on HST the ACS devices undergo a monthly annealing process. The TECs are turned off for 10 to 16 hours to allow the CCDs to warm up to ~19 C, a temperature high enough to break the bonds of the radiation damaged lattice and to allow reconstruction of the original structure during cool down. At the end of the annealing period, when the focal plane is brought back to its nominal temperature a series of dark frames is acquired. It is possible to measure the effectiveness of the anneal process by comparing two dark frames taken just before and after the thermal cycle. Transient hot pixels that after 6-7 anneal cycles do not recover their normal status remain permanently hot<sup>13</sup>. Therefore we can define two different rates of hot pixels growth, the daily growth of new hot pixels and the growth of permanent hot pixels. Figure 6 shows the evolution of hot pixels with dark current > 0.08 e-/pix/sec as a function of time for the CCD WFC-1 in ~ 100 days. New hot pixels in this signal range steadily develop at a rate of ~ 400 pixels per day in each

WFC chip (slope of segments B-B', C-C' and D-D'). No significant variations in the daily hot pixel growth have been observed in the first two years. After each anneal cycle, marked with a vertical dashed line in figure 6, the number of hot pixels created in the preceding months which maintain a dark current higher than the threshold decrease drastically. The anneal rate is given by the number of hot pixels that annealed away in a given month divided by the number of new hot pixels that grew in that month, for example  $(B'-C)/(B'-B)$ ,  $(C'-D)/(C'-C)$ , etc. in figure 6.



**Figure 6.** Plots of the total number of hot pixels vs. the day number for WFC1. The vertical dashed lines indicate the dates on which anneals occurred. The solid lines show the fit to the daily new hot pixels growth. The dotted line shows the permanent hot pixels growth.

We calculated the anneal rate in all three ACS CCDs and find that the anneal rate is strongly dependent on the threshold. After the initial 6-7 months the anneal rate remains constant. It takes a few months before the anneal process get in the full regime: new hot pixels generated in a given month and not annealed during the first thermal cycle still have a finite chance to get annealed within the following 6-7 cycles<sup>13</sup>. What we measure here is the net anneal rate of hot pixels before each anneal cycle. Figure 7 shows the average anneal rate for the two WFC and the HRC CCD as a function of the hot pixel threshold. In each device very hot pixels are annealed much better than the warm pixels. This behavior has also been reported from WFC3 radiation testing<sup>12,14</sup>. Depending on the threshold the anneal rate ranges from ~65 % to ~88 %. It should be remembered that WFC and HRC have a different operating temperature (-77 C and -81 C respectively) but they are annealed at the same temperature (~ +20 C).

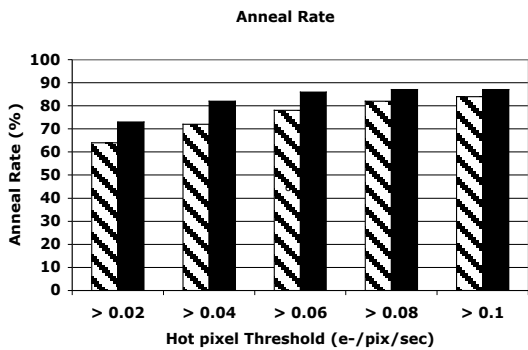


**Figure 7:** Anneal rate for WFC(dashed bars) and HRC CCDs (solid bars) as a function of the hot pixel signal level

annealing process is still not well understood, and its dependence on the annealing temperature and duration is still under investigation<sup>14</sup>.

A meaningful comparison between the anneal rate or the growth rate of hot pixels in different instruments is quite complex. Clearly operating temperature and threshold have a major impact on the results, but also annealing temperature and radiation shielding can play a role. In Table 5 we list the anneal rate for different instruments. Keeping in mind that the HRC and STIS CCDs are almost identical, that the focal plane housing was build from the same design, and that they are operated almost at the same temperature, we could conclude that new hot pixels with dark rate  $> 0.1$  e-/pix/hr are more likely to be annealed in the HRC CCD than in the STIS CCD. It should be noted, however, that the STIS annealing temperature is 15 C degree colder. The

Directly linked to the anneal rate, is the permanent hot pixels growth. This rate is calculated using the number of hot pixels in dark frames just after each anneal cycle (letters B,C,D and E in figure 6). At any threshold the number of permanent hot pixels in ACS CCDs increases linearly with time (figure 8). This trend is also observed in STIS<sup>15</sup>. The hot pixel population in WFPC2 CCDs shows

Instrument	Temp (CCD/ann.)	Threshold (e-/pix/sec)	Anneal rate	Reference
STIS orbit	- 83 / + 5	> 0.1	~ 80 % ~ 75 %	15,16
WFPC2 orbit	- 88 / + 22	> 0.02 <i>variable</i>	~ 80 %	17
WFC3 ground	- 83 / + 30	> 0.01 > 0.02 > 0.044	67 - 80 % ~ 80 % 93 - 97%	12,14

**Table 5:** Anneal rate for different instruments

different growth rates before and after the summer 1998, similarly to the temporal variation of the dark rate: the rate of creation of permanent hot pixels with dark current > 0.02 e-/pix/sec has decreased by a factor 3.

Table 6 lists the science impact of hot pixels, expressed as percentage of hot pixels that become permanently hot every year in different instruments. From this analysis results that at the same threshold STIS images suffer more from the hot pixel contamination than WFC or HRC.

Hot pixels could for the most part be eliminated by the superdark subtraction from science images. However, since the dark current in hot pixels is dependent on the signal level<sup>18</sup>, this process is not perfect. Moreover there are indications that the noise in hot pixels is much higher than the normal shot noise<sup>13</sup>. For these reasons the subtraction of a superdark frame from a science image cannot fully restore the ability to provide accurate flux measurements in hot pixels. The best strategy to reduce the scientific impact of hot pixels is to either the observations and discard the information on hot pixels during image combination.

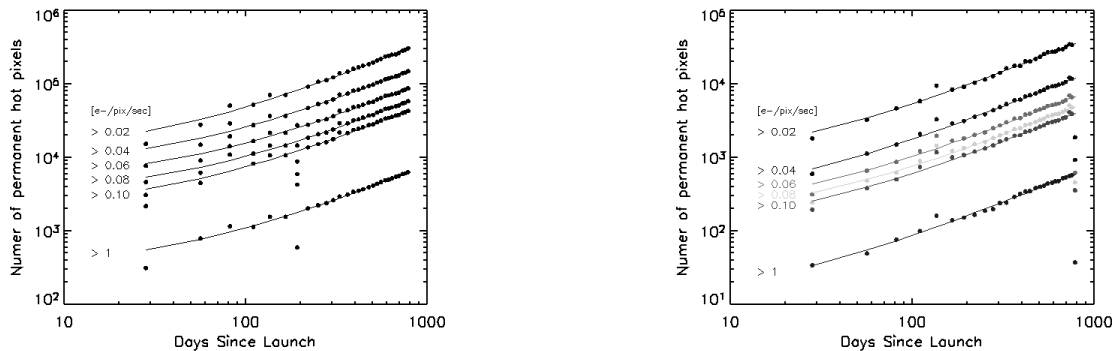


**Figure 8:** Permanent hot pixels growth with time for WFC (left) and HRC (right) for different signal levels.

Threshold e-/pix/sec	WFC	HRC	STIS	WFPC2
> 0.02	1.60	1.54	2.99	0.30 /0.11 <sup>a</sup>
>0.04	0.78	0.52		
>0.06	0.46	0.29		
>0.08	0.30	0.21		
>0.10	0.23	0.17	0.36	
>1	0.03	0.02	0.08	
temp	- 77 C	- 80 C	-83 C	- 88 C
Dark curr. e-/pix/sec	0.003	0.004	0.006	0.008

**Table 6:** Percent of pixels that became permanently hot every year for different thresholds and different instruments.  
a) before and after the summer 1998

Pixel Response (FPR) tests have been implemented in the ACS flight software. The CTE test campaign is executed twice a year covering a wide range of signal levels. Every month the EPER and FPR tests are executed on the WFC CCDs at a signal level of 1620e- to allow a direct comparison with the ground Fe<sup>55</sup> tests. Due to the design of the WFC CCDs, CTE measurement with EPER are possible in both the serial and parallel direction, whereas with the FPR is only possible to measure the serial CTE. Figure 7 shows the parallel CTE for WFC and HRC at several epochs. Just after on month in orbit (SMOV) the initial signs of CTE degradation were already visible for the very faint signal levels. The degradation at all signal levels is clearly progressing with time.

## 6. Charge Transfer Efficiency

CTE degradation is, without any doubt, the radiation damage effect that has largest impact on the scientific return of CCDs operated in a radiative environment. CTE degradation is due to charge trapping during the readout, and causes errors in stellar photometry, stellar astrometry and distortions in the observed surface brightness of extended objects. The CTE performance of the WFC detectors has been extensively measured on the ground in normal conditions, and after they have been radiated with 63MeV protons to a cumulative fluence that corresponds to 1, 2.5 and 5 years of exposure in the HST orbit<sup>5</sup>. On orbit, several calibration proposals measure the absolute value of the CTE, its degradation with time and the impact on the photometric accuracy of ACS. In particular Extended Pixel Edge Response (EPER) and First

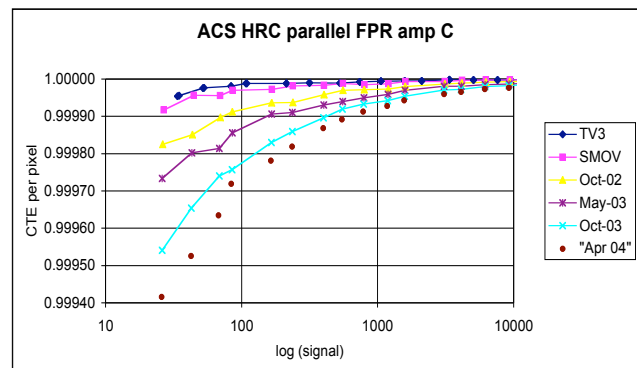
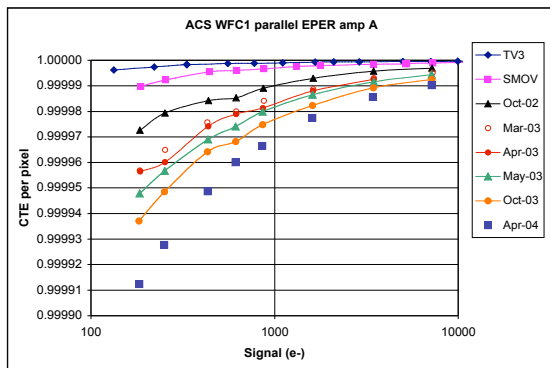


**Figure 7:** Eper parallel CTE for WFC (left) and FPR parallel CTE for HRC at different epochs.

If we compare the monthly measurement of the EPER parallel CTE for a signal level of 1620 e- in WFC detectors we can characterize the trend of the CTE degradation. Figure 8 shows that the measurements for WFC1 and WFC2 are in perfect agreement and that the CTE is degrading linearly with time. This trend is also observed at all the other signal levels and confirms ground testing predictions.

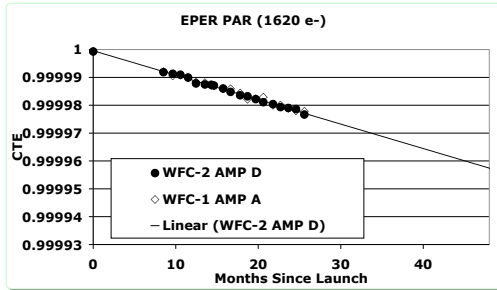


**Figure 8:** Eper CTE as a function of time for WFC1 and WFC2 at 1620e-.

comparison we use the “standard” signal level of 1620e-, which allows a direct comparison with the typical Fe<sup>55</sup> tests done during ground testing.

A corrective formula to apply to photometric measurements to remove the impact of CTE degradation has been derived by observation of a field of stars in 47 Tucanae<sup>18</sup>. This study shows that the current level of CTE degradation, still does not affect significantly the photometric performance of ACS. Only in the extreme case of a faint object with a weak background and located far from the readout amplifier, more than few percent of the flux is lost during the readout. The supplied formula provides the correction to apply to the observed magnitude to convert it to the magnitude the star would have in absence of CTE loss. This  $\Delta mag$  can be converted in CTE figure as  $10^{-(\Delta mag / (2.5 * n))}$  where n is the distance in pixels of the object from the serial register. Since the corrective formula for WFC<sup>18</sup> includes a time dependence, which confirms the linearity observed with the more traditional CTE tests, we can measure the rate of CTE degradation directly from photometric measurements. For this comparison we selected a star with a flux of 1620 e- over a background of 1 electron/pixel.

The monthly CTE degradation rates at a signal level of 1620e- for different tests are listed in table 7. The photometric test has been as “external”. At the moment it is not possible to make any comparison for the HRC results. When the photometric correction formula for the HRC parallel CTE will include a time dependence we will perform such a comparison. For the WFC parallel CTE, the EPER and External tests give a degradation rate in perfect agreement. The results of EPER and Fe<sup>55</sup> preflight testing on radiated parts are in agreement but they differ from the on-orbit figure. The ground measurements predict a more rapid parallel CTE deterioration than the observed one. A similar difference is present when comparing the degradation of the serial CTE. At least three factors should be taken into account when comparing ground predictions and on-orbit results: 1) there is a difference of ~ 5C degrees in the CCD operating temperature, the CCD being warmer on-orbit, 2) the parallel clocking has been slightly slowed down, no variations have been applied to the serial clocking and 3) during the pre-flight testing the CCDs were irradiated at room temperature without bias whereas on orbit the detectors are cold and constantly biased. More analysis is required before we can draw any firm conclusions. It is however likely, given the perfect agreement between the on-orbit tests, that the CTE degradation in ACS CCDs is proceeding slower than expected.

Camera	Direction	Test	Monthly CTE Degradation Rate	Temp	Notes
HRC	Parallel	Eper FPR	- 8 x 10 <sup>-7</sup> - 2 x 10 <sup>-6</sup>	-81 C	
WFC	Parallel	Eper External	- 7 x 10 <sup>-7</sup> - 6 x 10 <sup>-7</sup>	-77 C	Signal =1620 background=1e-
WFC Ground	Parallel	EPER Fe <sup>55</sup>	- 4 x 10 <sup>-6</sup> - 6 x 10 <sup>-6</sup>	-81 C	Slightly faster clocking
WFC	Serial	EPER	- 6 x 10 <sup>-8</sup>	-77 C	
WFC Ground	Serial	FPR Fe <sup>55</sup>	- 5 x 10 <sup>-7</sup>	-81 C	Same clocking

**Table 7:** Monthly CTE degradation rate from different tests on orbit and ground predictions.

The comparison of the results from different CTE tests with ground predictions presents several difficulties. First, different tests measure CTE in different ways, by calculating the amount of deferred charges (EPER, hot pixel tails) or trapped charges (FPR, Fe<sup>55</sup>). Second, the conditions between ground testing and on-orbit operation can be different. For example, temperature and clocking rate have a major impact on CTE performance of a CCD and often ground radiation testing are performed during the procurement phases when not all the conditions of on-orbit operation have been defined. So in order to compare the results from different tests, instead of the absolute CTE figure, we compare the rate of CTE degradation. For this

## 7. Conclusions

We investigated the performance of the ACS CCDs after two years on orbit. Their performances are affected by the ongoing damage due to the space radiation environment where they operate. The read noise in one of the four WFC amplifiers increased by  $\sim 0.7$  e- probably due to radiation damage in some electronic component. The dark rate is increasing at an average rate of 1.8 e-/pix/hr/yr in agreement with pre-flight predictions. Permanent hot pixels are developing at a steady rate. The effectiveness of the annealing process shows a strong dependence on the signal level: very hot pixels anneal better than warmer pixels. A direct comparison of the anneal rate is not without difficulties. The percentage of pixels that became permanently hot every year is slightly lower for HRC than WFC.

The current investigation of the CTE seems to suggest that the on-orbit CTE degradation is proceeding slower than expected. More analysis is required to confirm this result.

The comparison with other CCDs on board of HST shows that radiation-induced performance degradation in ACS CCDs is at the same level or slightly better than in STIS CCDs and WFPC2 CCDs. However, after  $\sim 5$  yr of operation on orbit the WFPC2 CCDs degradation significantly slowed down. A similar behavior has not been observed in the STIS CCD which has operated on orbit since 1997.

## Acknowledgements

ACS was developed under NASA contract NAS5-32864. The authors wish to thank J. Biretta, B. Hill, E. Polidan, A. Riess, R. van der Marel and the ACS IDT team for useful discussion and insight.

## 8. References

1. Ford, H. et al. 1996 "The Advanced Camera for the Hubble Space Telescope", in Space Telescopes and Instruments IV, Proc. SPIE, Vol. 2807, 184
2. Clampin, M. et al. 1998, "CCD Detectors for the HST Advanced Camera for Surveys", in Space Telescopes and Instruments V, eds. P.Y. Bely and J.B. Breckinridge, Proc. SPIE, Vol. 3356, 332
3. Sirianni M., et al 2002, "Characterization and Performance of ACS CCDs", in Future and UV Visible Space Astrophysics Missions and Instrumentation, eds. J.C. Blades & O.H. Siegmund, Proc. SPIE, Vol. 4854, 496
4. Tran, H.D et al. 2002 "On-orbit Performance of the ACS Solar Blind Channel", in Future and UV Visible Space Astrophysics Missions and Instrumentation, eds. J.C. Blades & O.H. Siegmund, Proc. SPIE, Vol. 4854, 686
5. Ford H, et al. 2002 "Overview of the Advanced Camera for Surveys On-orbit Performance", in Future EUV and UV Visible Space Astrophysics Missions and Instrumentation, eds. J. C. Blades & O.H. Siegmund, Proc. SPIE, Vol. 4854, 81
6. Sirianni M., et al 2003 "Characterization and on-orbit performance of the Advanced Camera for Surveys CCDs" in Future EUV/UV and Visible Space Astrophysics Missions and Instrumentation. Edited by J. Chris Blades, Oswald H. W. Siegmund. Proceedings of the SPIE, Volume 4854, pp. 496
7. Clampin M., et al . 2004 "Inflight performance of the Advanced Camera for Surveys" in Focal Plane Arrays for Space Telescopes. Edited by Grycewicz, Thomas J.; McCreight, Craig R. Proceedings of the SPIE, Volume 5167, pp. 235
8. Mutchler, M. et al. 2004 HST-ACS ISR 2004-07
9. Sirianni M. et al 2004 HST-ACS ISR in preparation
10. Brown, T. M., 2001, HST-STIS ISR 2001-003.
11. Mack, J., et l. 2001, HST-WFPC2 ISR 2001-05.
12. Polidan E. et al. 2004 "Hot pixel behavior in WFC3 CCD detectors irradiated under operational conditions" in Focal Plane Arrays for Space Telescopes. Edited by Grycewicz, Thomas J.; McCreight, Craig R. Proceedings of the SPIE, Volume 5167, pp. 258
13. Riess, A., 2002 HST-ACS ISR 2002-09
14. Polidan, E. et al 2004 SPIE 5487 in preparation
15. Hayes et al. 1998 HST-STIS ISR 98-06-revision A
16. Kim Quijano, J. et al. STIS Instrument Handbook 2003- STScI
17. Koekemoer A. et al. WFPC2 Instrument Handbook 2003- STScI
18. Riess, A. et al. 2004 HST-ACS ISR 2004-06
19. Mutchler et al. 2004 HST-ACS ISR in preparation
20. Waczynski, A. et al. 2001. "A comparison of CTE measurement Techniques on Proton Damaged n-channel CCDs for the Hubble Space Telescope Wide-Field Camera 3", IEEE Trans. On Nuclear Science, Vol 48, N. 6, pag 1807.